Ocean Heat Content responses to changing Anthropogenic Aerosol Forcing Strength: regional and multi-decadal variability

Emma J.D. Boland[1,1,1,1], Andrea J. Dittus[2,2,2,2], Daniel C Jones[1,1,1,1], Simon A. Josey[3,3,3,3], and Bablu Sinha[4,4,4,4]

[1]British Antarctic Survey
[2]University of Reading
[3]National Oceanography Centre
[4]National Oceanography Centre, Southampton

December 8, 2022

Abstract

The causes of decadal variations in global warming are poorly understood, however it is widely understood that variations in ocean heat content are linked with variations in surface warming. To investigate the forced response of ocean heat content (OHC) to anthropogenic aerosols (AA), we use an ensemble of historical simulations, which were carried out using a range of anthropogenic aerosol forcing magnitudes in a CMIP6-era global circulation model. We find that the centennial scale linear trends in historical ocean heat content are significantly sensitive to AA forcing magnitude (\$-3.0\pm0.1\$ x10\$ˆ{5}\$ (J m\$ˆ{-3}\$ century\$ˆ{-1}\$)/(W m\$ˆ{-2}\$), R\$ˆ2\$=0.99), but interannual to multi-decadal variability in global ocean heat content appear largely independent of AA forcing magnitude. Comparison with observations find consistencies in different depth ranges and at different time scales with all but the strongest aerosol forcing magnitude, at least partly due to limited observational accuracy. We find broad negative sensitivity of ocean heat content to increased aerosol forcing magnitude across much of the tropics and sub-tropics. The polar regions and North Atlantic show the strongest heat content trends, and also show the strongest dependence on aerosol forcing magnitude. However, the ocean heat content response to increasing aerosol forcing magnitude in the North Atlantic and Southern Ocean is either dominated by internal variability, or strongly state dependent, showing different behaviour in different time periods. Our results suggest the response to aerosols in these regions is a complex combination of influences from ocean transport, atmospheric forcings, and sea ice responses.

Table 2. Linear correlations between changes in volume-scaled Ocean Heat Content 20-year means, from 1850-1870 to 1995-2015, and present day aerosol forcing magnitude, split by depth range and basin. R^2 indicates the square of the Pearson correlation coefficient, with bold indicating statistical significance at the 99% level. Slope indicates the slope of the linear fit, in units of 10^5 J/m^3/century/(W m^{-2}).

		Global	Atlantic	Pacific	Southern	Indian
Full Depth	R^2	0.99	0.94	0.98	0.96	0.95
	Slope	[illegible]	[illegible]	[illegible]	[illegible]	[illegible]
0-300m	R^2	0.98	0.99	0.96	0.86	0.96
	Slope	[illegible]	[illegible]	[illegible]	[illegible]	[illegible]
300-700m	R^2	0.97	0.97	0.94	0.87	0.87
	Slope	[illegible]	[illegible]	[illegible]	[illegible]	[illegible]
700-2000m	R^2	0.94	0.71	0.95	0.70	0.86
	Slope	[illegible]	[illegible]	[illegible]	[illegible]	[illegible]
2km+	R^2	0.04	0.69	0.45	0.74	0.27
	Slope	[illegible]	[illegible]	[illegible]	[illegible]	[illegible]

individual basins and depth ranges indicate the relative importance of non-linear impacts and feedbacks on other forcings on OHU and transport for these sub-domains.

The strength of the relationship (indicated by the slope of the linear fit) is strongest for the Atlantic at all depths. In the deep ocean (2km+), the Atlantic and Southern OHC fits are similar in strength but opposite in sign — the 2km+ Atlantic OHC is the only volume to show a *positive* relationship between OHC and AA 2014 ERF magnitude, indicating increased AA forcing increases deep Atlantic OHC. This is linked with changes in the Atlantic Meridional Overturning Circulation (AMOC), as discussed in section 3.2.3. The Global deep ocean shows no significant linear relation with AA 2014 ERF on a centennial timescale, due to the Southern OHC, and, to a lesser extent, the Indian and Pacific OHC, which have *negative* linear relations with AA 2014 ERF magnitude, acting in combination to offset the Atlantic relation of the opposite sign.

While the linear fits show that the magnitude of trends in OHC on centennial scales are sensitive to aerosol forcing magnitude, there is considerable non-linear behaviour in many basins and at many depth ranges at decadal scales (figure 1). This is investigated further in the following section.

3.1.2 Centennial scale changes: non-linear analysis

In order to assess the sensitivity of multi-decadal variability in OHC to AA forcing magnitude, we fit a polynomial to the full-depth global and basin-wise OHC anomaly time series (figures 1a-e). The degree of polynomial was chosen by experimenting with different degrees and choosing the lowest order fit (to favour simplicity and avoid overfit) that provided a relatively small residual (at least one order of magnitude smaller than the fit). A fourth order polynomial fits these criteria well for global OHC and basin-wise OHCs (figures 2a-e), with multi-decadal variability captured by the polynomial fits and residuals an order of magnitude smaller (figures 2f-k).

To determine the dependence of the multi-decadal variability on AA forcing magnitude, we perform a principal component analysis over the multi-ensemble dimension

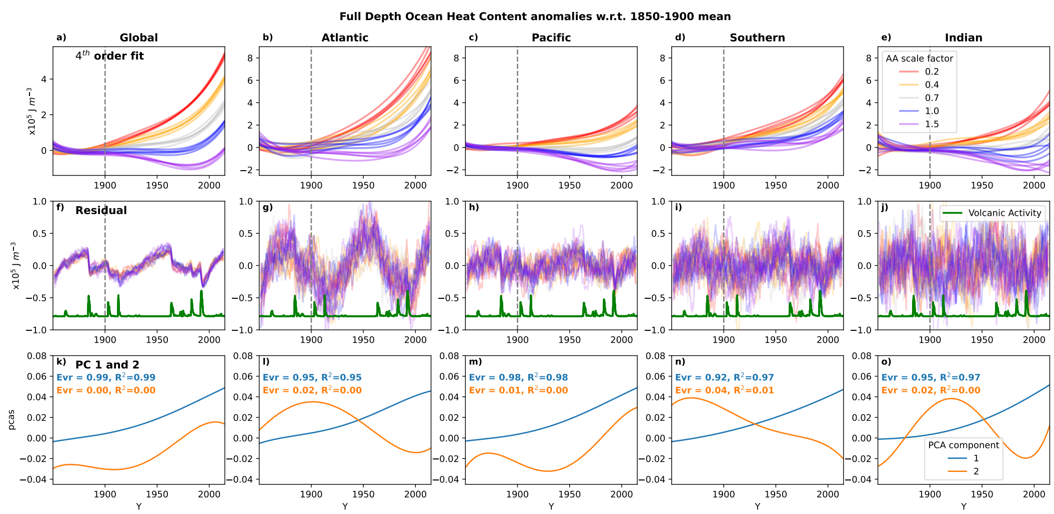

Figure 2. Multi-decadal linear trends are sensitive to AA factor, but annual to decadal variability is largely independent of AA forcing magnitude. Panels a-e show 4 th order polynomial ts to ocean heat content anomalies w.r.t. 1850-1900 ensemble means, globally and by basin (gures 1a-e), for all ensemble members. Colours indicates the AA forcing factor (see legend). Panels f-j show the residual ocean heat content, calculated by subtracting the 4th order ts (a-e) from the same ocean heat content anomalies, and smoothed with an 18 month low-pass Butterworth lter. The green line is a proxy for volcanic forcing, which is the same for all ensemble members, see text for details. Panels k-o show the form of the rst and second principal components of the 4th order ts in a-e. The explained variance (Evr) and correlations of the PC weights with AA ERF (R^2) are shown in each panel.

of the 25 polynomial time series shown in figures 2a-e. The form of the first and second principal components for the global and basin-wise polynomial fits are shown in figures 2k-o. The analysis indicates differences in multi-decadal linear trends between ensemble members is driven almost entirely by differences in aerosol forcing magnitude: The first PCs (blue lines) take the form of multi-decadal linear trends, explain 99% of the global variance (and at least 92% in the basins), and the weights of the first PCs are extremely significantly correlated with AA forcing magnitude for all basins and globally ($R^2 > :$). Indeed the form of the first PC resembles the form of the effective radiative forcing time series, which shows an increasing positive trend towards the end of the time period (Dittus et al., 2020). The ERF time series includes all forcings, with the prominent increase in the ERF time series primarily due to GHGs. The overall shape of PC1 mainly reflects the impact of GHG forcing, while the fact that the weights are highly correlated with the AA ERF indicates that the time series is modulated by AA.

Differences in multi-decadal non-linear variability, represented by the second PC (orange lines in figures 2k-o), are responsible for very little of the differences between the OHC time series, explaining maximum 4% of the variance, and the weights of the second PC are not significantly correlated with AA forcing magnitude (R^2). This indicates that AA forcing magnitude does not drive differences in multi-decadal non-linear variability in large scale OHC, and therefore differences in multi-decadal non-linear variability are driven by other forcing factors (kept constant in these ensembles).

Differences across the scaling ensembles in the residuals (figures 2f-k) are small, indicating that sub-decadal OHC variability (as defined here by the residuals of the 4^{th} order polynomial fit) is not primarily driven by differences in AA forcing magnitude in this model. Small/some differences on these timescales may exist (e.g. following volcanic eruptions) but are not investigated further here.

Sharp drops in residual OHC are associated with spikes in volcanic activity (figures 2, thick green lines), consistent with Church et al. (2005); Gleckler et al. (2006). Additionally, there is a circa 70 year periodic feature in the global OHC residual, also apparent in the Atlantic and Pacific OHCs to lesser degrees. These could be the result of a fitting artefact, or indicative of residual modes of multi-decadal internal variability such as the Atlantic Multidecadal Oscillation (AMO) (Deser et al., 2010) and/or the Interdecadal Pacific Oscillation (Parker et al., 2007), although it should be noted that Mann et al. (2021) argue that the AMO is entirely driven by volcanic forcing and not internally generated. The amplitude of the periodic feature is small compared with the multi-decadal variability in the polynomial fits, so we have not investigated further.

Using a LOWESS fit instead as in Cheng et al. (2022, not shown) results in a smaller magnitude residual and a different form of PC2, but does not change the form of PC1 or subsequent interpretation.

3.2 Ocean Heat Content Trends

Time series of Ocean Heat Content trends were calculated from the un-scaled global OHC as defined in equation 1 (without the factor $=V$ to allow for easier comparison with observations) as follows: At each time series point, a centred 30 year linear regression was calculated. For the model OHC, we used the $linregress$ function from the scipy python library (Virtanen et al., 2020). For the observed OHC, we used the WLS function from the statsmodels python library (Seabold & Perktold, 2010), with the weights$= = {}^2_E$, where ${}_E$ is the standard error provided with the observations. Both functions provided a standard error in the linear slope, as well as the slope itself.

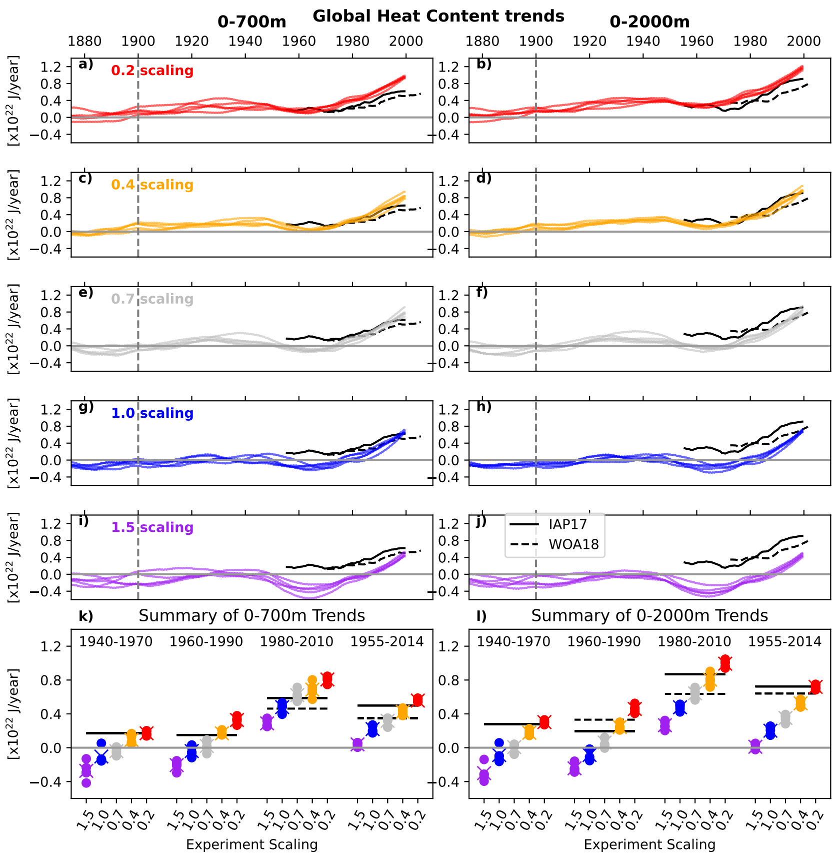

Figure 3. Observations of OHC trends are inconsistent with the 1.5 forcing factor for the period 1980-2010, and with both 1.0 and 1.5 for the periods 1940-1970 and 1960-1990. Panels a-j show OHC trends over time, by ensemble member (colour) and depth range 0-700m (a,c,e,g,i) or 0-2000m (b,d,f,h,j). The black solid lines are derived from ocean heat content observations from IAP17, the black dotted lines from WOA18. Panels k and l summarise the upper panels by taking data points from three, 30-year periods (1940-1970, 1960-1990, 1980-2010), as well as for one 70-year period covering 1955-2014. Coloured dots indicate ensemble members, coloured crosses ensemble means, and black lines observations as before.

3.2.1 Ocean Heat Content trends vs observations

In order to compare our modelled OHC with those from observations (WOA18 and IAP17, see section 2 for details), we calculated OHC trends for 0-700m and 0-2000m. Absolute values of simulated OHC are less likely to match observations, and the uncertainty in observations increases at earlier times due to measurement sparsity, whereas trends have relatively lower uncertainty, even when taking the uncertainty at individual times into account. The standard error provided with the observational datasets do not take into account all sources of uncertainty (Wang et al., 2018; Carton & Santorelli, 2008), and so we show two different products to indicate the magnitude of additional uncertainty.

The time series of simulated OHC trends (coloured lines, figures 3a-j) and observed trends (black solid and dashed lines, figures 3a-j) have standard errors one or two orders of magnitude (respectively) smaller than the OHC trends themselves, and so are not shown.

Both 0-700m and 0-2000m simulated OHC trends drop to a local minimum at around 1965 (representing the trend for 1950-1981), even becoming negative for the larger forcing factors, indicating ocean heat loss from these depth ranges to either the atmosphere or greater depths. This corresponds to the period with the greatest increase in aerosols (Dittus et al., 2020). From 1965 on, OHC trends for both depth ranges increase for all forcing factors, peaking at the end of the simulation. This is consistent with the form of the GMST time series in Dittus et al. (2020), which show faster than observed warming from 1990 onwards. Dittus et al. (2020) suggest this could indicate a possible warm bias in the transient climate response (TCR) of the model.

The observational OHC trends vary less than the simulated OHC trends: both are relatively flat until around 1970-1990, when they begin to increase, with the IAP17 dataset beginning to rise before the WOA18 dataset in both depth ranges (figures 3a-j). The 0.4 and 0.7 scaling trends show the most similarity to one or other of the observations for many decades in both depth ranges. The 0.2 and 1.0 scaling trends show some similarity at the start or ends of the observational time series. The 1.5 scaling trends are the only to not match observations in any time period or depth range. This is summarised in figures 3k and l, which show the linear trends for 1940-1970, 1960-1990, 1980-2010, and a single 70-year trend for 1955-2014.

Overall, the observations imply a scaling of 0.2-0.7 for the periods 1940-1980. From 1980 onwards, the 0-700m observations imply a scaling of 0.4-1.0, and the 0-2000m observations imply a scaling of 0.2-0.7. This is consistent with the results of Dittus et al. (2020), who also find the 0.4 and 0.7 scaling simulations match observations of global mean surface temperature, even when accounting for the warm bias in the model's TCR.

Anthropogenic aerosols are not evenly distributed around the planet (Stern, 2006), thus changes in the forcing factor will amplify/dampen regional differences and the resultant impacts on OHC. To further investigate the regional sensitivity of ocean heat content to aerosol forcing magnitude, we look at spatial patterns in both latitude/longitude (section 3.2.2) and latitude/depth (section 3.2.3).

3.2.2 Depth-integrated Ocean Heat Content trends

To investigate the spatial distribution of OHC trends in the SMURPHS ensemble,we calculate the depth-integrated OHC as follows:

$$_{xy} \qquad ; \qquad c_p \; _0\!\int \; dz; \qquad\qquad (2)$$

where $\int dz$ indicates an integral over the full depth of the model.

Figure 4. Spatial patterns of depth-integrated OHC trends vary by ensemble member, by AA forcing factor, and time period. Colours indicate the ensemble mean depth-integrated OHC for each forcing factor for (a) 1960-1991 and (b) 1980-2011. Grey contours indicate the ensemble standard deviation, at 2, 4 and 6 x10^7 J/m^2/year.

Figure 5. Patterns of zonally-integrated OHC vary by ensemble member, by AA forcing factor, and time period: Colours indicate the ensemble mean OHC_{yz} trends for each forcing factor for (a) 1960-1991 and (b) 1980-2011. Grey contours indicate the ensemble standard deviations at 2, 3.5, and 5 $\times 10^{11}$ J/m^2/year (a) and 2, 4, and 6 $\times 10^{11}$ J/m^2/year (b). Note that depth intervals are not constant, and colour axis limits in b) are twice those in a).

Figure 7. The sensitivity of Ocean Heat Content trends to aerosol forcing magnitude varies with basin, depth, and time period: Colours indicate the regression of a) 1960-1991 or b) 1980-2011 $O\hat{H}C_{yz}$ trends on 2014 AA ERF magnitude for all 25 ensemble members. Stippling indicates where the trend is statistically signi cant using the student T-test. Note that depth intervals are not constant.

in the Atlantic), and highly variable (figure 6), all likely due the additional impacts of heat convergence/divergence. The increased vertical transport in these regions leads to a stronger impact of aerosol forcing changes at depths (figure 7).

Thus, while we expect the impact of aerosols on ocean heat content to be non-uniform spatially, we might expect that the impact is similar at different times. In fact, we find that the regional impacts can vary significantly with time period. We focus in this paper on two 30-year periods near the end of the historical simulation (1960-1991, 1980-2011), both because they are the time periods with most observations and because the model behaviour is different in both periods - 1980-2011 sees a strong acceleration of global warming with subsequent impacts on cryosphere (Dittus et al., 2020; Andrews et al., 2020), shows a reversal in the trend in Atlantic Multidecadal Variability (AMV) (see Andrews et al. (2020) and figure S8), an increase in the trend of equivalent radiative forcing from all sources (Dittus et al., 2020), although there are significant regional variations (Dittus et al., 2022) and the overall AA forcing is stable in this period. Indeed, Andrews et al. (2020) link the change in AMV (and AMOC) trend sign in the standard historical forcing simulation (our 1.0 forcing case) with regional variations in aerosol forcing. We now discuss the differences between the two forcing periods and how they compare with literature for each basin in turn, with the Indian and Pacific basins discussed together.

4.2.1 Atlantic

Atlantic OHC shows the strongest relative response to increased AA ERF in both time periods by all measures presented - on a centennial, basin-integrated scale (table 2), and on a multi-decadal scale in both depth-integrated (figure 6) and zonally-integrated (figure 7) trends.

We find that the strength of the AMOC is dependent on aerosol ERF strength (figure S8). Additionally, there is a significant relationship between the centennial trend in AMOC strength and AA ERF (not shown), consistent with the results of Collier et al. (2013); Cai et al. (2006); Shi et al. (2018); Irving et al. (2019); Menary et al. (2020); Robson et al. (2022). However, there is not a clear link on shorter timescales - the links between the thirty-year trends in AMOC and AA ERF strength are not significant for 1960-1991 and of opposite sign to 1980-2011 (see figures S8f,g). The statistical correlations are also weak and of similar magnitude to internal variability, implying either multi-decadal variability in AMOC strength is not strongly controlled by AAs or that the processes are more complex than a correlation can represent. We hypothesise that AA regional trends rather than absolute AA forcing strength could influence AMOC strength: we see a centennial scale strengthening in the AMOC alongside increasing AA forcing up until circa. 1980, at which point regional decreases in AA across Europe and N America from 1980 onwards (strongest in the 1.5x scenario), alongside a sharp rise in GHGs, drive a decreasing AMOC (strongest in the 1.5x scenario).

The strengthening of the AMOC with increased AA forcing is consistent with the significant positive sensitivity of depth-integrated OHC in the Sub-Polar North Atlantic to AA ERF magnitude in 1960-1991. A similar pattern is seen in the depth-integrated temperature-trend response in Cai et al. (2006) (their figure 4), and the SST responses in Collier et al. (2013); Shi et al. (2018); Robson et al. (2022). This pattern is consistent with the increased convergence of heat in the region, which Shi et al. (2018); Robson et al. (2022) find leads to increased heat loss to the atmosphere, decreasing upper ocean stratification and further strengthening the AMOC. This feedback effect may explain the link between centennial AMOC trends and AA ERF magnitude.

During the period 1980-2011, we still see relatively strong cooling in the south Atlantic in response to increased AA forcing magnitude, but we no longer see warming south of Greenland (figure 6b). Instead, the regression in this region resembles the pattern of OHC trends in the simulations (figure 4), with a ‘warming hole’ south of Greenland, linked in Liu et al. (2020) to a slowing of the AMOC, consistent with the weak dependence of AMOC trend on AA forcing magnitude in this time period (figure S7g). We still see an increase in warming at depth in the north Atlantic (figure 7b) but the upper ocean heat content response to increased aerosols appears to be under the influence of multiple interacting and possible competing processes - a strengthened but decreasing AMOC, a strong slowing in the loss of Arctic sea ice (Dittus et al., 2020), and changes in NH aerosol composition with North American and European emissions dropping against a background of increasing Asian emissions (Dittus et al., 2022).

4.2.2 Indo-Pacific

In the Pacific, Cai et al. (2006) find the inclusion of aerosols in historic gcm simulations induce a cross-equatorial overturning circulation, with northward transport at the surface and southward transport down to circa 800m depth, inducing warming north of the equator and cooling south of it. This resembles the pattern of OHC sensitivity to aerosol forcing magnitude in 1960-1981, both depth-integrated (figure 6a) and zonally integrated (figure 7c), although the latter is not statistically significant. In 1980-2011 the Pacific regression pattern is instead dominated by a PDO-like signal, linked by Dittus et al. (2022) to a surface pressure response to increased aerosol forcing, possibly triggered by a Rossby wave response to increased Asian aerosol emissions since the 1980s.

Sun et al. (2022) find that a weakened AMOC leads to compensating northward transport in the Indo-Pacific basins, causing heat to be redistributed from the Atlantic to the Indo-Pacific basins via the Southern Ocean, leading to sub-surface (1-3km) warming. The implied opposite effect due to the AMOC strengthening is consistent with the sub-surface negative sensitivity in both the Pacific and Indian basins here.

Whilst the Pacific doesn't stand out when comparing the relative sensitivity of OHC to AAs between basins, it is the largest basin and contributes the most in absolute terms to the sensitivity of global OHC to AAs [not shown]. Thus, the Pacific's broad statistically significant negative sensitivity to AAs (see figure 6) indicate it plays an important role in the ocean's energy budget during the historical period.

4.2.3 Southern Ocean

Whilst the Southern Ocean is far from the strongest aerosol forcing locations, it is clear that its dominant role in ocean heat storage is significantly dependent on aerosol forcing magnitude. Especially notable is during 1960-1991, when GHG forcing is relatively weaker than in 1980-2011, the strongest aerosol forcings (1.0 and 1.5) lead to a cooling in much of the upper 2000m in the Southern Ocean (see figure 5a).

The warming at depth to the north of the Southern Ocean in both time periods in response to increased AA ERF magnitude is likely linked to the strengthening of the global meridional overturning circulation, as indicated by the changes in the AMOC discussed above.

In the Southern Ocean in 1960-1991 (figure 7e), we see a cooling pattern that is the opposite of the GHG-induced trends in Southern ocean heat storage (Liu et al., 2018; Dias et al., 2020) - surface cooling north of 55S and a concentration of statistically significant cooling at 40S-45S in the upper 1000m due to weakening of the overturning circulation and a reduction in heat convergence. This is consistent with a negative SAM-like pattern in the regression of SLP against aerosol forcing found in this time period in Dittus et al. (2022) (although not statistically significant), implying decreasing zonal winds. However, Steptoe et al. (2016) find a similar negative response in the SAM to AA changes in CMIP5 models is not robust and model-dependent.

In 1980-2011, we instead see a concentration of surface cooling at 60S, and less relative cooling in the interior. This could be due to the contribution of warming at these latitudes in the Indian sector (figure 6b). This may also be influenced by the positive SAM-like response to aerosol forcing in this time period (Dittus et al., 2022), which acts to increase the wind-induced overturning circulation, strengthening the GHG induced effects and relatively warming the interior, although there is still a cooling effect of aerosol forcing overall. Additionally, there is an increased loss of Antarctic sea ice extent in the model in 1981-2011 in both summer and winter (see figure S9), which is slowed by increased aerosol forcing when considering the ensemble means, although there is large internal variability. Increased sea ice cover is consistent with relative cooling at the surface close to the continent, whilst the warming at depth below is consistent with the production of cold, dense waters slowing (figure 7f).

5 Summary

Using a unique ensemble of 25 simulations of the historical climate with five different anthropogenic aerosol forcing time series, we have been able to determine the influence of aerosol forcing magnitude on ocean heat content in a CMIP6-era gcm. We find that the 20th century volume-scaled global ocean heat uptake sensitivity to anthropogenic aerosol forcing magnitude is : $\hat{d}$: x10^5 (J m^{-3} century^{-1})/(W m^{-2}) for the HadGEM3-GC3.1-LL model. Centennial changes in the OHC of the major ocean basins and globally integrated depth ranges above 2000m also show significant linear dependence on AA forcing magnitude (R^2 0.94), indicating that the impact of non-linear effects and feedbacks from other forcings are negligible. We find that aerosol forcing magnitude is responsible for changes in multi-decadal global ocean heat content linear trends at global and basin-wide scales (R^2 :), but that interannual to multi-decadal variability is relatively insensitive to forcing magnitude.

Trends in 0-700m ocean heat content are most consistent with observations for the 0.4-1.0 scaling experiments, consistent with Dittus et al. (2020), who find the 0.4 and 0.7 scaling experiments most consistent with GMST observations. Trends in 0-2000m ocean heat content are most consistent with observations for the 0.2-0.7 experiments. Both results are consistent with Robson et al. (2022), who find that CMIP6 models with the strongest aerosol forcings are inconsistent with observations.

We find the responses to increased anthropogenic aerosol strength is significantly dependent on region and time period. In general, the strongest responses are found in the regions where there are the strongest trends in OHC, specifically the North Atlantic and Southern Oceans. The responses in these regions are summarised in figure 8, with proposed mechanisms.

The difference in aerosol sensitivity in the different time periods implies a strong state dependence of the aerosol impacts on OHC, such that the impact of aerosols forcing changes on OHC is different depending on a combination of some or all of: the ocean, atmosphere, and cryosphere state; the magnitude and distributions of other forcings (GHGs, volcanic, natural aerosols); the magnitude of the aerosol forcing itself (the ERF is generally higher and increasing for all forcing factor experiments in 1980-2011 compared with 1960-1991, see Dittus et al. (2020) figure 1b).

Our results give, for the first time, a well-constrained estimate of the dependence of historic global ocean heat uptake on aerosol forcing magnitude. Our results suggest that ocean heat content could potentially be used to constrain the estimate of the true aerosol forcing magnitude, but that accurate and sustained measurements would be required.

We find that there is significant regional and decadal variability in the sensitivity of ocean heat content to aerosol forcing magnitude in regions of high ocean heat uptake.

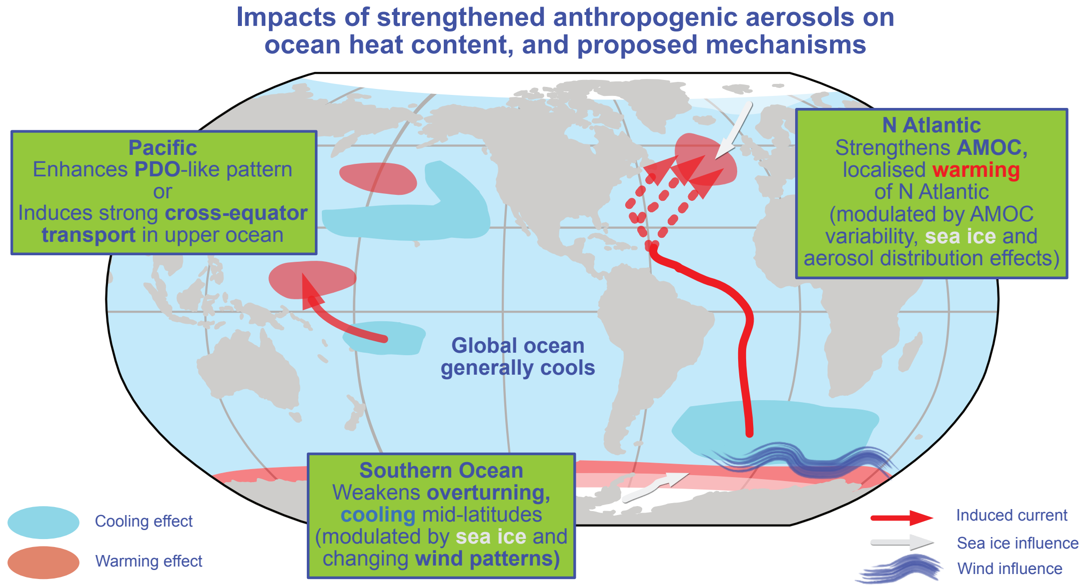

Figure 8. Schematic outlining the impacts of increasing anthropogenic aerosol forcing magnitude on historic ocean heat content in a CMIP6-era global climate model, with proposed mechanisms.

The uncertainty in aerosol forcing magnitude is not the dominant source of regional variability - instead the strong state dependence means that careful process based studies are required to disentangle the various mechanisms at play that determine the overall regional impact of aerosol forcing in di erent time periods.

6 Appendix

Appendix A Drivers of Changes in Ocean Heat Content

Ocean heat uptake (OHU) is de ned as the globally integrated ocean temperature trend, i.e. the trend in global OHC. In a climate at equilibrium, time-integrated OHU would tend to zero. A non-zero time-integrated OHU is therefore due, at rst order, to changes in the major climate forcings - green-house gases (GHGs), anthropogenic aerosols (AA), volcanic and other natural aerosols (NA) - as well as internal variability (IV) and feedbacks proportional to atmospheric temperatures T:

$$f \qquad g \qquad h \qquad :T; \qquad \text{(A1)}$$

where $f; g; h$ are functions representing the impact of the relevant processes on OHU, and the strength of temperature feedbacks. If we hold GHG and NA levels constant (as in the SMURPHS ensemble), and look at su ciently long timescales, then we can estimate the linear sensitivity of OHU to AA:

$$\frac{}{} \qquad \frac{@ \qquad =@t}{} \quad g \qquad ; \qquad \text{(A2)}$$

neglecting higher order terms, where averaging over ensemble members removes the impact of internal variability.

However, if we look at trends of OHC over a sub-domain, for example a single basin or depth range, or integrated in one or two spatial dimensions only, then the trend in

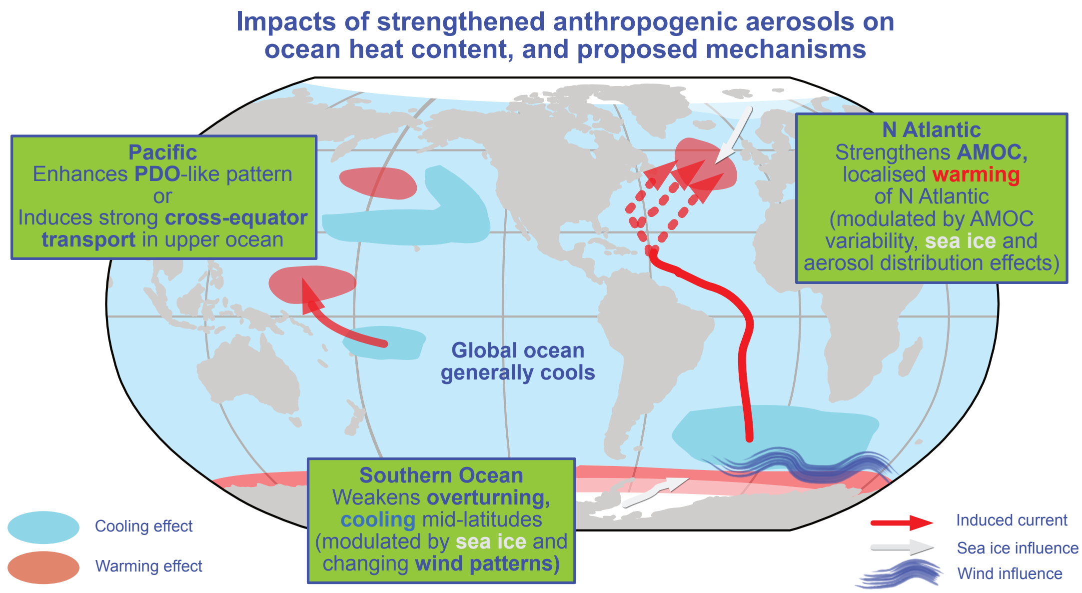

Figure 8. Schematic outlining the impacts of increasing anthropogenic aerosol forcing magnitude on historic ocean heat content in a CMIP6-era global climate model, with proposed mechanisms.

The uncertainty in aerosol forcing magnitude is not the dominant source of regional variability - instead the strong state dependence means that careful process based studies are required to disentangle the various mechanisms at play that determine the overall regional impact of aerosol forcing in different time periods.

6 Appendix

Appendix A Drivers of Changes in Ocean Heat Content

Ocean heat uptake (OHU) is defined as the globally integrated ocean temperature trend, i.e. the trend in global OHC. In a climate at equilibrium, time-integrated OHU would tend to zero. A non-zero time-integrated OHU is therefore due, at first order, to changes in the major climate forcings - green-house gases (GHGs), anthropogenic aerosols (AA), volcanic and other natural aerosols (NA) - as well as internal variability (IV) and feedbacks proportional to atmospheric temperatures T:

$$f \qquad g \qquad h \qquad :T; \qquad \text{(A1)}$$

where $f; g; h$ are functions representing the impact of the relevant processes on OHU, and the strength of temperature feedbacks. If we hold GHG and NA levels constant (as in the SMURPHS ensemble), and look at sufficiently long timescales, then we can estimate the linear sensitivity of OHU to AA:

$$\frac{\text{Q}}{\int} \qquad \frac{\text{Ŧ} \; @ \qquad =@t}{\int} \quad g \qquad ; \qquad \text{(A2)}$$

neglecting higher order terms, where averaging over ensemble members removes the impact of internal variability.

However, if we look at trends of OHC over a sub-domain, for example a single basin or depth range, or integrated in one or two spatial dimensions only, then the trend in

OHC (sometimes termed ocean heat storage, OHS) has contributions from both OHU and the convergence or divergence of ocean heat transport:

$$\frac{\partial}{\partial t} \qquad : \quad ; \tag{A3}$$

Thus, changes in the OHC of sub-domains are not solely determined by climate forcings and their feedbacks, but also depend on ocean circulation changes in response to AA. Again, if looking at su ciently long timescales and neglecting higher order terms,:

$$\frac{\varrho}{\int} \quad g_r \quad \frac{\partial}{\partial} \quad : \tag{A4}$$

where g_r represents the regional impact of AA on OHU.

Acknowledgments

DJ was supported by UK Research and Innovation grant (MR/T020822/1). DJ, SJ, and BS were funded by the UK Natural Environment Research Council ACSIS program (NE/N018028/1 and NE/N018044/1). EB, AD and the SMURPHS ensemble were funded by the Natural Environment Research Council (grants NE/N006186/1 and NE/N006054/1), and the ensemble was also supported by the National Centre for Atmospheric Science.

The data required to reproduce the gures and tables in this manuscript is held at `https://doi.org/10.6084/m9.figshare.19281761` (Boland et al., 2022).

The code to reproduce the gures and tables, as well as to produce the intermediate data from the model output, is held at `https://doi.org/10.5281/zenodo.6418479` (Boland, 2022).

References

Andrews, M. B., Ridley, J. K., Wood, R. A., Andrews, T., Blockley, E. W., Booth, B., ... others (2020). Historical simulations with hadgem3-gc3. 1 for cmip6. *Journal of Advances in Modeling Earth Systems*, *12*(6), e2019MS001995.

Bellouin, N., Quaas, J., Gryspeerdt, E., Kinne, S., Stier, P., Watson-Parris, D., ... others (2020). Bounding global aerosol radiative forcing of climate change. *Reviews of Geophysics*, *58*(1), e2019RG000660.

Boland, E. (2022, November). *emmomp/smurphs_ ohc: Third release.* Zenodo. Retrieved from `https://doi.org/10.5281/zenodo.7382823` doi: 10.5281/zenodo.7382823

Boland, E., Jones, D., Dittus, A., Josey, S., & Sinha, B. (2022, Nov). *Smurphs ohc data.* gshare. Retrieved from `https://doi.org/10.6084/m9.figshare.19281761` doi: 10.6084/m9. gshare.19281761

Booth, B. B., Dunstone, N. J., Halloran, P. R., Andrews, T., & Bellouin, N. (2012). Aerosols implicated as a prime driver of twentieth-century north atlantic climate variability. *Nature*, *484*(7393), 228 232.

Booth, B. B., Harris, G. R., Jones, A., Wilcox, L., Hawcroft, M., & Carslaw, K. S. (2018). Comments on rethinking the lower bound on aerosol radiative forcing . *Journal of Climate*, *31*(22), 9407 9412.

Boucher, O., Randall, D., Artaxo, P., Bretherton, C., Feingold, G., Forster, P., ... others (2013). Climate change 2013: the physical science basis. Contribution of Working Group I to the Fifth Assessment Report of the Intergovernmental Panel on Climate Change. *K., Tignor, M., Allen, SK, Boschung, J., Nauels, A., Xia, Y., Bex, V., and Midgley, PM, Cambridge University Press, Cambridge, UK*.

Boyer, T. P., Garcia, H. E., Locarnini, R. A., Zweng, M. M., Mishonov, A. V., Reagan, J. R., ... Smolyar, I. V. (2018). *World Ocean Atlas 2018.*

NOAA National Centers for Environmental Information. Retrieved from https://accession.nodc.noaa.gov/NCEI-WOA18 (Ocean Heat Content Datasets, accessed July 2021)

Cai, W., Bi, D., Church, J., Cowan, T., Dix, M., & Rotstayn, L. (2006). Pan-oceanic response to increasing anthropogenic aerosols: Impacts on the southern hemisphere oceanic circulation. *Geophysical research letters*, *33*(21).

Carton, J. A., & Santorelli, A. (2008). Global decadal upper-ocean heat content as viewed in nine analyses. *Journal of Climate*, *21*(22), 6015 6035.

Chen, X., & Tung, K.-K. (2014, aug). Varying planetary heat sink led to global-warming slowdown and acceleration. *Science*, *345*(6199), 897 903. doi: 10.1126/science.1254937

Cheng, L., Foster, G., Hausfather, Z., Trenberth, K. E., & Abraham, J. (2022). Improved quanti cation of the rate of ocean warming. *Journal of Climate*, 1 37.

Cheng, L., Trenberth, K. E., Fasullo, J., Boyer, T., Abraham, J., & Zhu, J. (2017). Improved estimates of ocean heat content from 1960 to 2015. *Science Advances*, *3*(3), e1601545.

Church, J. A., White, N. J., & Arblaster, J. M. (2005, nov). Signi cant decadal-scale impact of volcanic eruptions on sea level and ocean heat content. *Nature*, *438*(7064), 74 77. doi: 10.1038/nature04237

Collier, M. A., Rotstayn, L. D., Kim, K.-Y., Hirst, A. C., & Je rey, S. J. (2013). Ocean circulation response to anthropogenic-aerosol and greenhouse gas forcing in the csiro-mk3. 6 coupled climate model. *Aust. Meteorol. Oceanogr. J*, *63*, 27 39.

Delworth, T. L., Ramaswamy, V., & Stenchikov, G. L. (2005, dec). The impact of aerosols on simulated ocean temperature and heat content in the 20th century. *Geophysical Research Letters*, *32*(24), L24709. doi: 10.1029/2005GL024457

DesbruyŁres, D. G., Purkey, S. G., McDonagh, E. L., Johnson, G. C., & King, B. A. (2016). Deep and abyssal ocean warming from 35 years of repeat hydrography. *Geophysical Research Letters*, *43*(19), 10 356.

Deser, C., Alexander, M. A., Xie, S.-P., & Phillips, A. S. (2010). Sea surface temperature variability: Patterns and mechanisms. *Annual review of marine science*, *2*, 115 143.

Dias, F. B., Fiedler, R., Marsland, S., Domingues, C., ClØment, L., Rintoul, S., ... Savita, A. (2020). Ocean heat storage in response to changing ocean circulation processes. *Journal of Climate*, *33*(21), 9065 9082.

Dittus, A. J., Hawkins, E., Robson, J. I., Smith, D. M., & Wilcox, L. J. (2022). Drivers of recent North Paci c decadal variability: the role of aerosol forcing. *Earth's Future*, *Under Review*.

Dittus, A. J., Hawkins, E., Wilcox, L. J., Sutton, R. T., Smith, C. J., Andrews, M. B., & Forster, P. M. (2020, jul). Sensitivity of Historical Climate Simulations to Uncertain Aerosol Forcing. *Geophysical Research Letters*, *47*(13). doi: 10.1029/2019GL085806

Ekman, A. M. (2014, Jan). Do sophisticated parameterizations of aerosol-cloud interactions in CMIP5 models improve the representation of recent observed temperature trends? *Journal of Geophysical Research: Atmospheres*, *119*(2), 817 832. doi: 10.1002/2013JD020511

England, M. H., McGregor, S., Spence, P., Meehl, G. A., Timmermann, A., Cai, W., ... Santoso, A. (2014, mar). Recent intensi cation of wind-driven circulation in the Paci c and the ongoing warming hiatus. *Nature Climate Change*, *4*(3), 222 227. doi: 10.1038/nclimate2106

Fiedler, S., & Putrasahan, D. (2021, apr). How Does the North Atlantic SST Pattern Respond to Anthropogenic Aerosols in the 1970s and 2000s? *Geophysical Research Letters*, *48*(7), e2020GL092142. doi: 10.1029/2020GL092142

Forster, P., Storelvmo, T., Armour, K., Collins, W., Dufresne, J.-L., Frame, D., ... Zhang, H. (2021). Climate Change 2021: The Physical Science Basis.

Contribution of Working Group I to the Sixth Assessment Report of the Intergovernmental Panel on Climate Change. In (chap. The Earth's Energy Budget, Climate Feedbacks, and Climate Sensitivity). Cambridge University Press. (In Press)

Fyfe, J. C., Meehl, G. A., England, M. H., Mann, M. E., Santer, B. D., Flato, G. M., . . . Swart, N. C. (2016). Making sense of the early-2000s warming slowdown. *Nature Climate Change*, *6*(3), 224 228. doi: 10.1038/nclimate2938

Gleckler, P. J., AchutaRao, K., Gregory, J. M., Santer, B. D., Taylor, K. E., & Wigley, T. M. L. (2006, sep). Krakatoa lives: The e ect of volcanic eruptions on ocean heat content and thermal expansion. *Geophysical Research Letters*, *33*(17), L17702. doi: 10.1029/2006GL026771

Hobbs, W., Palmer, M. D., & Monselesan, D. (2016, mar). An Energy Conservation Analysis of Ocean Drift in the CMIP5 Global Coupled Models. *Journal of Climate*, *29*(5), 1639 1653. doi: 10.1175/JCLI-D-15-0477.1

Hoesly, R. M., Smith, S. J., Feng, L., Klimont, Z., Janssens-Maenhout, G., Pitkanen, T., . . . others (2018). Historical (1750 2014) anthropogenic emissions of reactive gases and aerosols from the Community Emissions Data System (CEDS). *Geoscientific Model Development*, *11*(1), 369 408.

Irving, D., Wij els, S., & Church, J. (2019). Anthropogenic aerosols, greenhouse gases, and the uptake, transport, and storage of excess heat in the climate system. *Geophysical Research Letters*, *46*(9), 4894 4903.

Jones, G. S., Stott, P. A., & Christidis, N. (2013, May). Attribution of observed historical near surface temperature variations to anthropogenic and natural causes using CMIP5 simulations. *Journal of Geophysical Research: Atmospheres*, *118*(10), 4001 4024. doi: 10.1002/JGRD.50239

Kosaka, Y., & Xie, S.-P. (2013, sep). Recent global-warming hiatus tied to equatorial Paci c surface cooling. *Nature*, *501*(7467), 403 407. doi: 10.1038/nature12534

Levitus, S., Antonov, J. I., Boyer, T. P., Baranova, O. K., Garcia, H. E., Locarnini, R. A., . . . others (2012). World ocean heat content and thermosteric sea level change (0 2000 m), 1955 2010. *Geophysical Research Letters*, *39*(10).

Liu, W., Fedorov, A. V., Xie, S.-P., & Hu, S. (2020). Climate impacts of a weakened Atlantic Meridional Overturning Circulation in a warming climate. *Science Advances*, *6*(26), eaaz4876. doi: 10.1126/sciadv.aaz4876

Liu, W., Lu, J., Xie, S.-P., & Fedorov, A. (2018, jun). Southern Ocean Heat Uptake, Redistribution, and Storage in a Warming Climate: The Role of Meridional Overturning Circulation. *Journal of Climate*, *31*(12), 4727 4743. doi: 10.1175/JCLI-D-17-0761.1

Mann, M. E., Steinman, B. A., Brouillette, D. J., & Miller, S. K. (2021). Multidecadal climate oscillations during the past millennium driven by volcanic forcing. *Science*, *371*(6533), 1014 1019. doi: 10.1126/science.abc5810

Marshall, J., Scott, J. R., Armour, K. C., Campin, J.-M., Kelley, M., & Romanou, A. (2015, apr). The ocean's role in the transient response of climate to abrupt greenhouse gas forcing. *Climate Dynamics*, *44*(7-8), 2287 2299. doi: 10.1007/s00382-014-2308-0

Meehl, G. A., Arblaster, J. M., Fasullo, J. T., Hu, A., & Trenberth, K. E. (2011, oct). Model-based evidence of deep-ocean heat uptake during surface-temperature hiatus periods. *Nature Climate Change*, *1*(7), 360 364. doi: 10.1038/nclimate1229

Menary, M. B., Robson, J., Allan, R. P., Booth, B. B., Cassou, C., Gastineau, G., . . . others (2020). Aerosol-forced amoc changes in cmip6 historical simulations. *Geophysical Research Letters*, *47*(14), e2020GL088166.

Meyssignac, B., Boyer, T., Zhao, Z., Hakuba, M. Z., Landerer, F. W., Stammer, D., . . . Zilberman, N. (2019, aug). Measuring Global Ocean Heat Content to Estimate the Earth Energy Imbalance. *Frontiers in Marine Science*, *6*(JUL),

432. doi: 10.3389/fmars.2019.00432
Oka, A., & Watanabe, M. (2017, apr). The post-2002 global surface warming slowdown caused by the subtropical Southern Ocean heating acceleration. *Geophysical Research Letters*, *44*(7), 3319 3327. doi: 10.1002/2016GL072184
Parker, D., Folland, C., Scaife, A., Knight, J., Colman, A., Baines, P., & Dong, B. (2007). Decadal to multidecadal variability and the climate change background. *Journal of Geophysical Research: Atmospheres*, *112*(D18).
Purkey, S. G., & Johnson, G. C. (2010). Warming of global abyssal and deep southern ocean waters between the 1990s and 2000s: Contributions to global heat and sea level rise budgets. *Journal of Climate*, *23*(23), 6336 6351.
Qin, M., Dai, A., & Hua, W. (2020). Aerosol-forced multidecadal variations across all ocean basins in models and observations since 1920. *Science advances*, *6*(29), eabb0425.
Robson, J., Menary, M. B., Sutton, R. T., Mecking, J., Gregory, J. M., Jones, C., . . . Wilcox, L. J. (2022). The role of anthropogenic aerosol forcing in the 1850 1985 strengthening of the amoc in cmip6 historical simulations. *Journal of Climate*, *1*(aop), 1 48.
Seabold, S., & Perktold, J. (2010). statsmodels: Econometric and statistical modeling with python. In *9th python in science conference.*
Shi, J. R., Xie, S. P., & Talley, L. D. (2018, sep). Evolving Relative Importance of the Southern Ocean and North Atlantic in Anthropogenic Ocean Heat Uptake. *Journal of Climate*, *31*(18), 7459 7479. doi: 10.1175/JCLI-D-18-0170.1
Smith, C. J., Kramer, R. J., Myhre, G., Alterskjæ, K., Collins, W., Sima, A., . . . Forster, P. M. (2020). E ective radiative forcing and adjustments in CMIP6 models. *Atmospheric Chemistry and Physics*, *20*(16), 9591 9618. doi: 10.5194/acp-20-9591-2020
Steptoe, H., Wilcox, L. J., & Highwood, E. J. (2016, sep). Is there a robust e ect of anthropogenic aerosols on the southern annular mode? *Journal of Geophysical Research*, *121*(17), 10029 10042. doi: 10.1002/2015JD024218
Stern, D. I. (2006). Reversal of the trend in global anthropogenic sulfur emissions. *Global Environmental Change*, *16*(2), 207 220.
Stolpe, M. B., Cowtan, K., Medhaug, I., & Knutti, R. (2021, jan). Paci c variability reconciles observed and modelled global mean temperature increase since 1950. *Climate Dynamics*, *56*(1-2), 613 634. doi: 10.1007/s00382-020-05493-y
Sun, S., Thompson, A. F., Xie, S.-P., & Long, S.-M. (2022). Indo-paci c warming induced by a weakening of the atlantic meridional overturning circulation. *Journal of Climate*, *35*(2), 815 832.
Virtanen, P., Gommers, R., Oliphant, T. E., Haberland, M., Reddy, T., Cournapeau, D., . . . SciPy 1.0 Contributors (2020). SciPy 1.0: Fundamental Algorithms for Scienti c Computing in Python. *Nature Methods*, *17*, 261 272. doi: 10.1038/s41592-019-0686-2
Wang, G., Cheng, L., Abraham, J., & Li, C. (2018). Consensuses and discrepancies of basin-scale ocean heat content changes in di erent ocean analyses. *Climate dynamics*, *50*(7), 2471 2487.
Wilcox, L. J., Highwood, E. J., & Dunstone, N. J. (2013, jun). The in uence of anthropogenic aerosol on multi-decadal variations of historical global climate. *Environmental Research Letters*, *8*(2), 024033. doi: 10.1088/1748-9326/8/2/024033
Yin, J., Overpeck, J., Peyser, C., & Stou er, R. (2018, jan). Big Jump of Record Warm Global Mean Surface Temperature in 2014 2016 Related to Unusually Large Oceanic Heat Releases. *Geophysical Research Letters*, *45*(2), 1069 1078. doi: 10.1002/2017GL076500
Zanna, L., Khatiwala, S., Gregory, J. M., Ison, J., & Heimbach, P. (2019, jan). Global reconstruction of historical ocean heat storage and transport. *Proceedings of the National Academy of Sciences*, *116*(4), 1126 1131. doi:

10.1073/pnas.1808838115

Supporting Information for "Ocean Heat Content responses to changing Anthropogenic Aerosol Forcing Strength: regional and multi-decadal variability"

Emma J.D. Boland[1], Andrea J. Dittus[2], Daniel C. Jones[1], Simon A. Josey[3],

and Bablu Sinha[3]

[1]British Antarctic Survey, Cambridge, UK

[2]National Centre for Atmospheric Science, University of Reading, Reading, UK

[3]National Oceanography Centre, Southampton, UK

Contents of this file

Introduction The supplementary information contains figures that there was not space for in the main manuscript, or that provide more granularity than the figures in the main manuscript. All figures are referenced in the main manuscript.

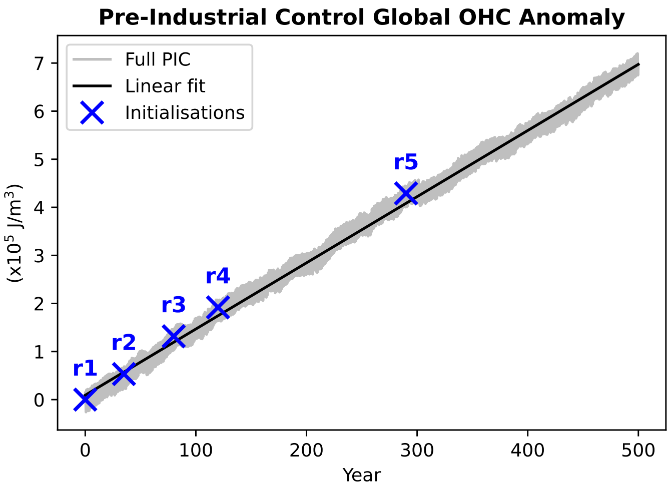

Figure S1. Example of Pre-Industrial Control drift in OHC: Global OHC anomalies from the Pre-Industrial Control Run, scaled by volume as outlined in main text (grey line), linear fit used to de-drift (black line), and locations of initialisations for each ensemble member of the historical simulations (blue crosses). De-drifting involved removing the 500-yr linear trend (black line) and accounting for the separation of the initialisations (different crosses).

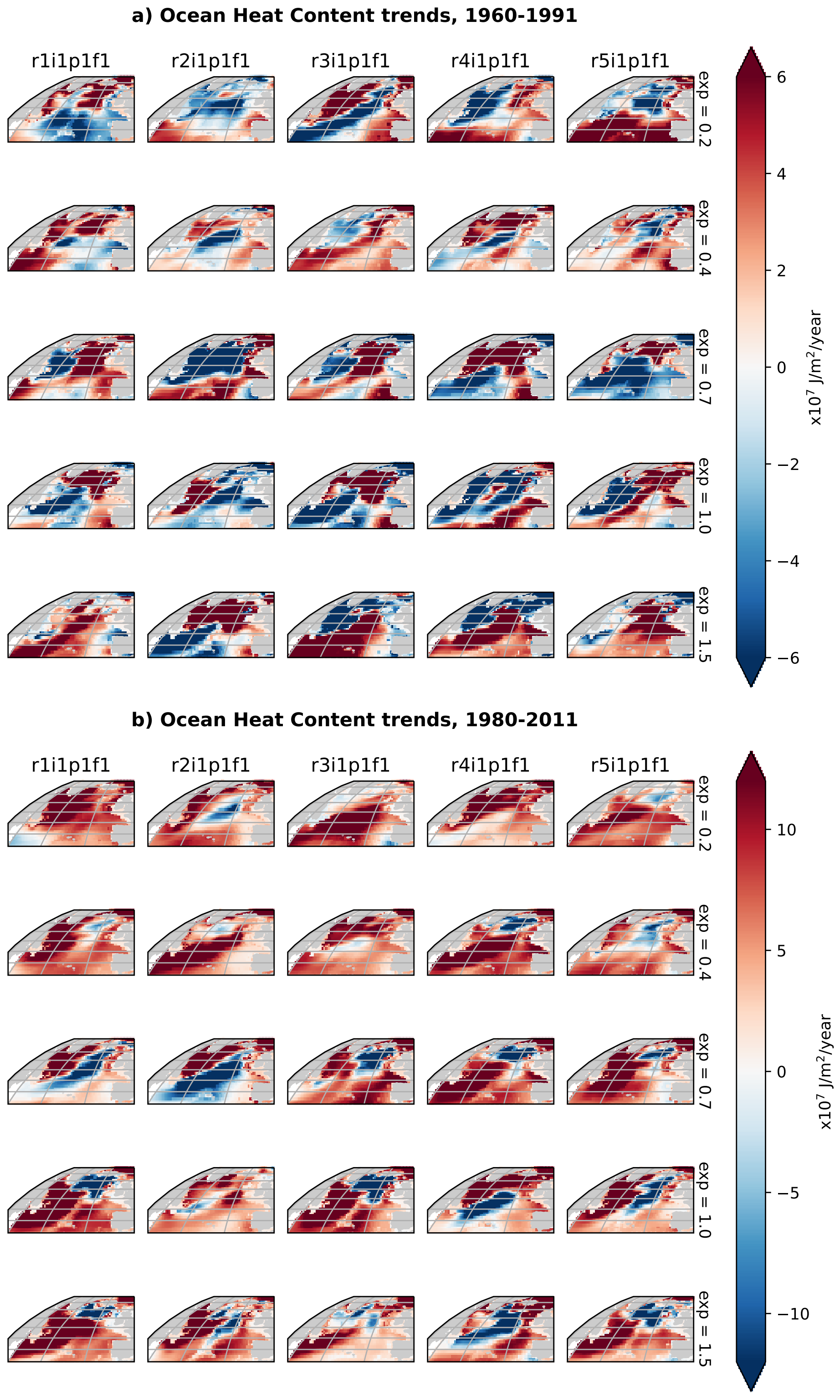

Figure S2. Colours indicate the North Atlantic depth-integrated OHC trends by ensemble member (column) and by AA forcing factor (row) as labelled, for (a) 1960-1991 and (b) 1980-2011.

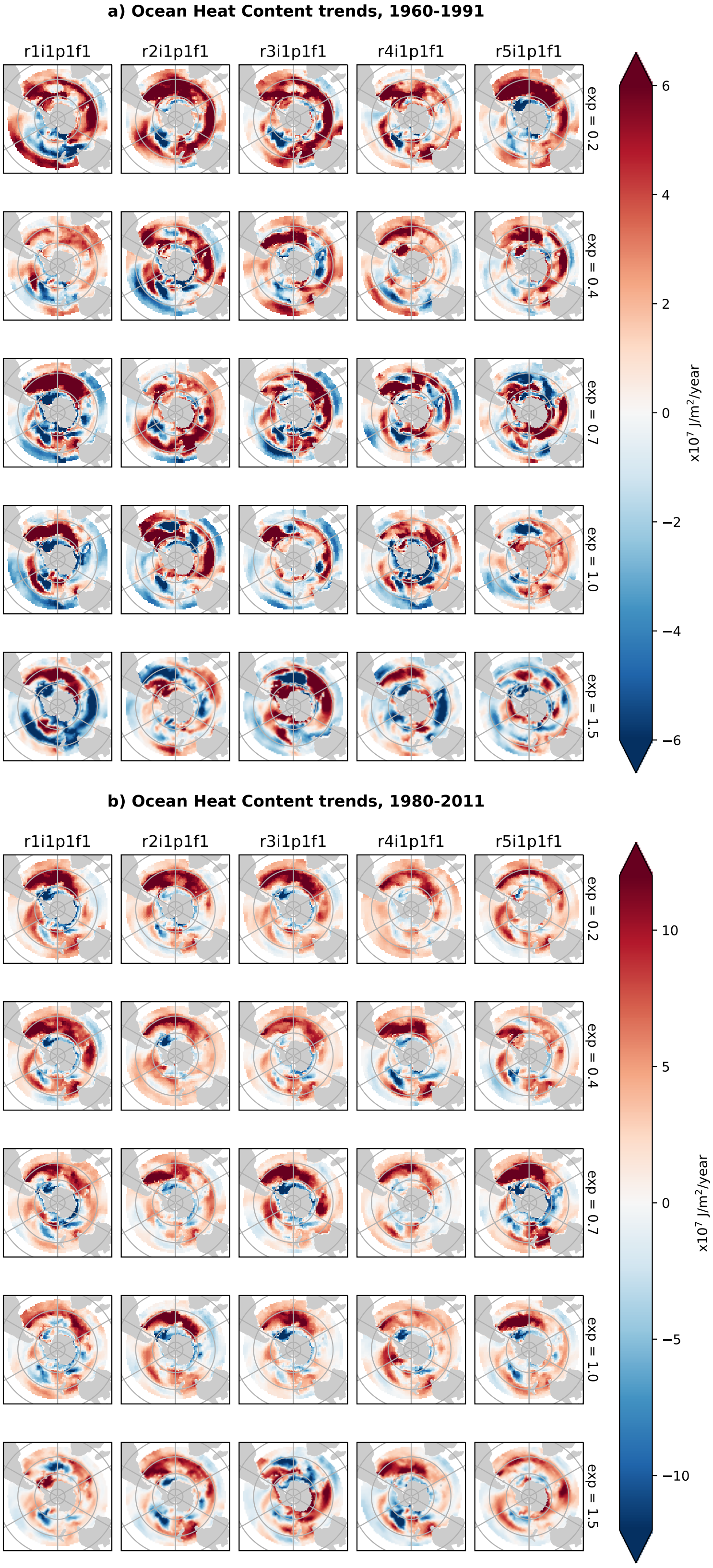

Figure S3. As in figure S1, but for the Southern Ocean

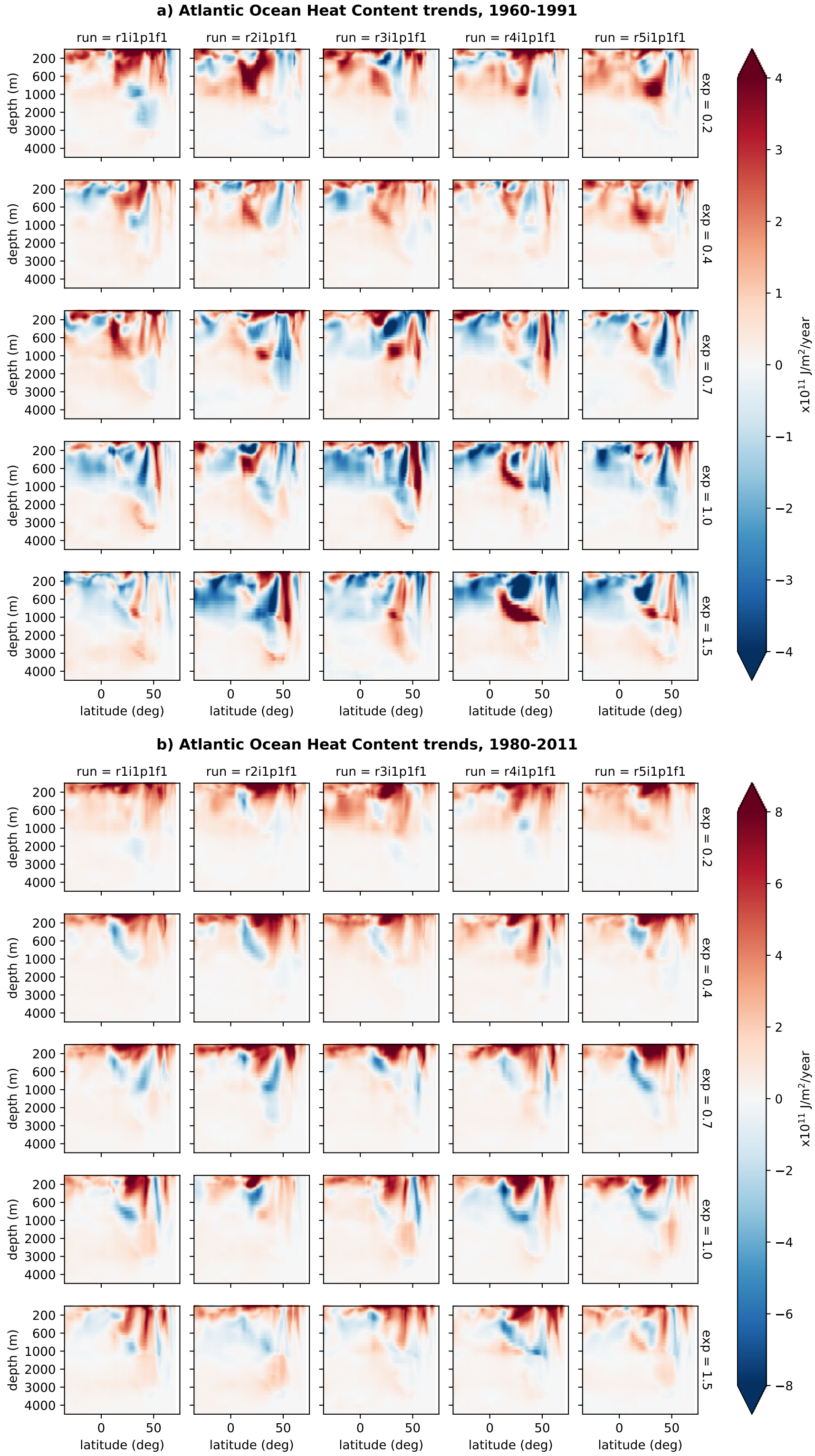

Figure S4. Colours indicate the zonally-integrated Atlantic OHC trends for each ensemble member (column) and each forcing factor (row) for (a) 1960-1991 and (b) 1980-2011. Note that depth intervals are not constant, and colour axis limits in b) are twice those in a).

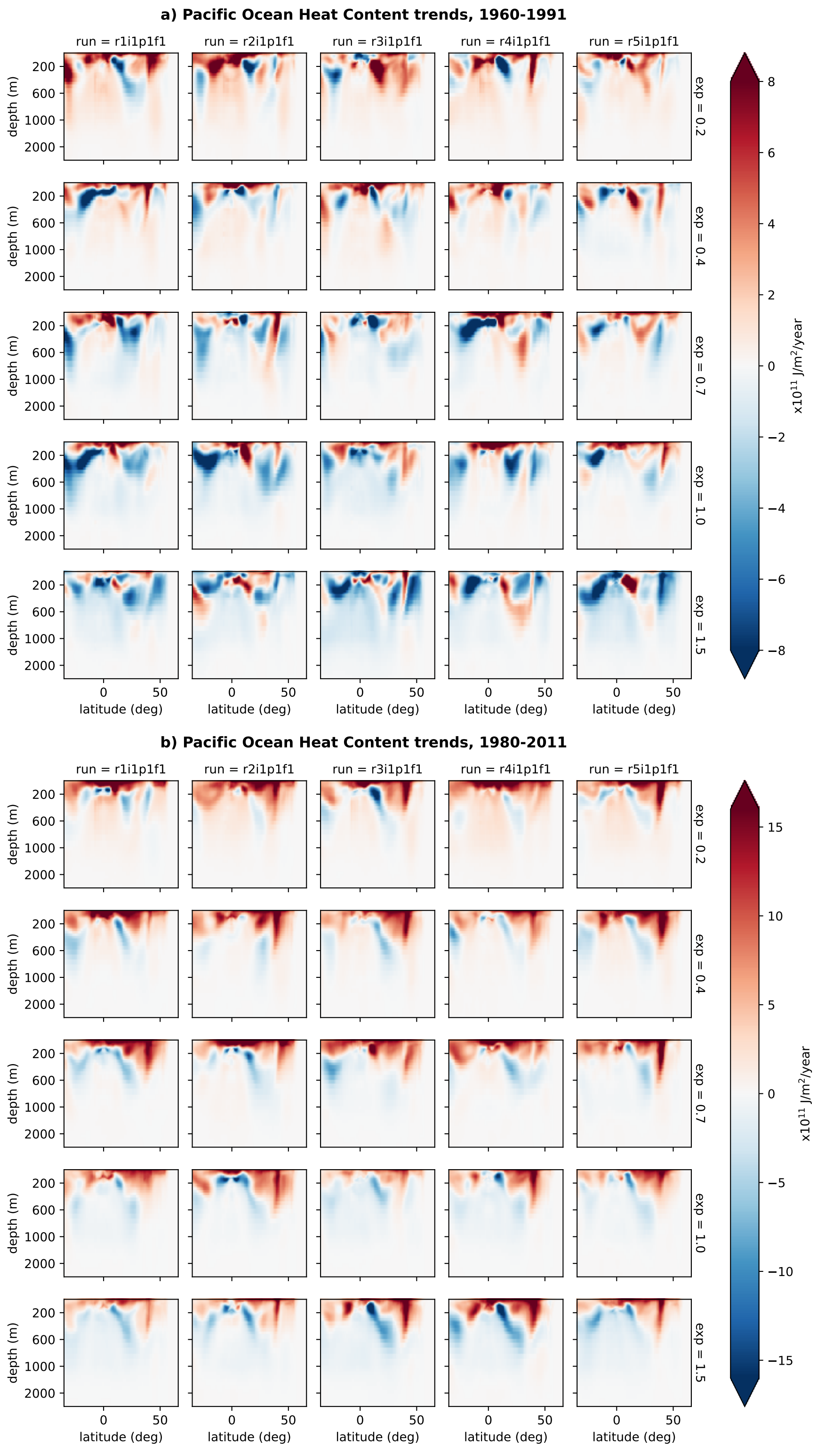

Figure S5. As in figure S3, except for the Pacific Ocean.

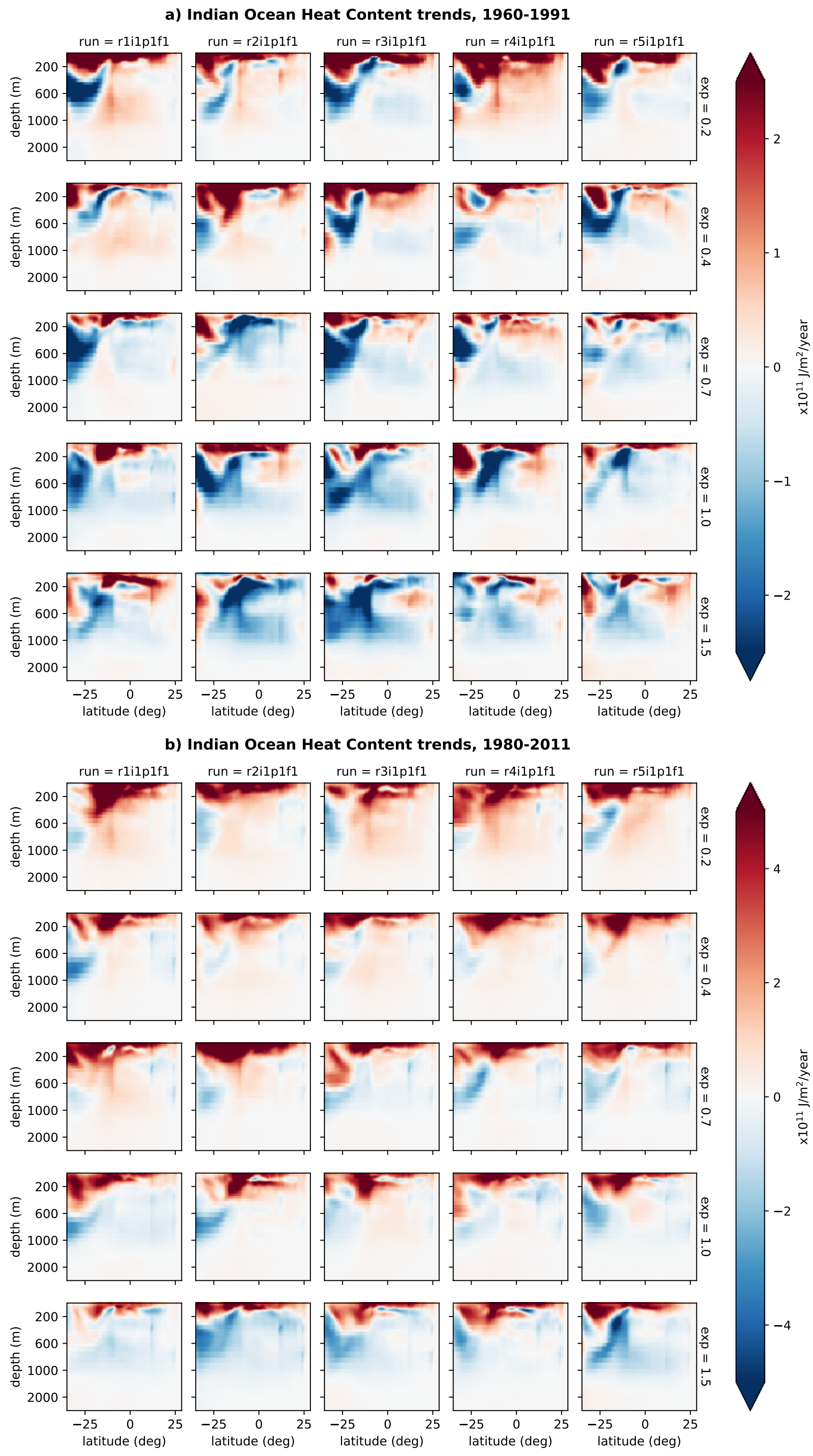

Figure S6. As in figure S3, except for the Indian Ocean.

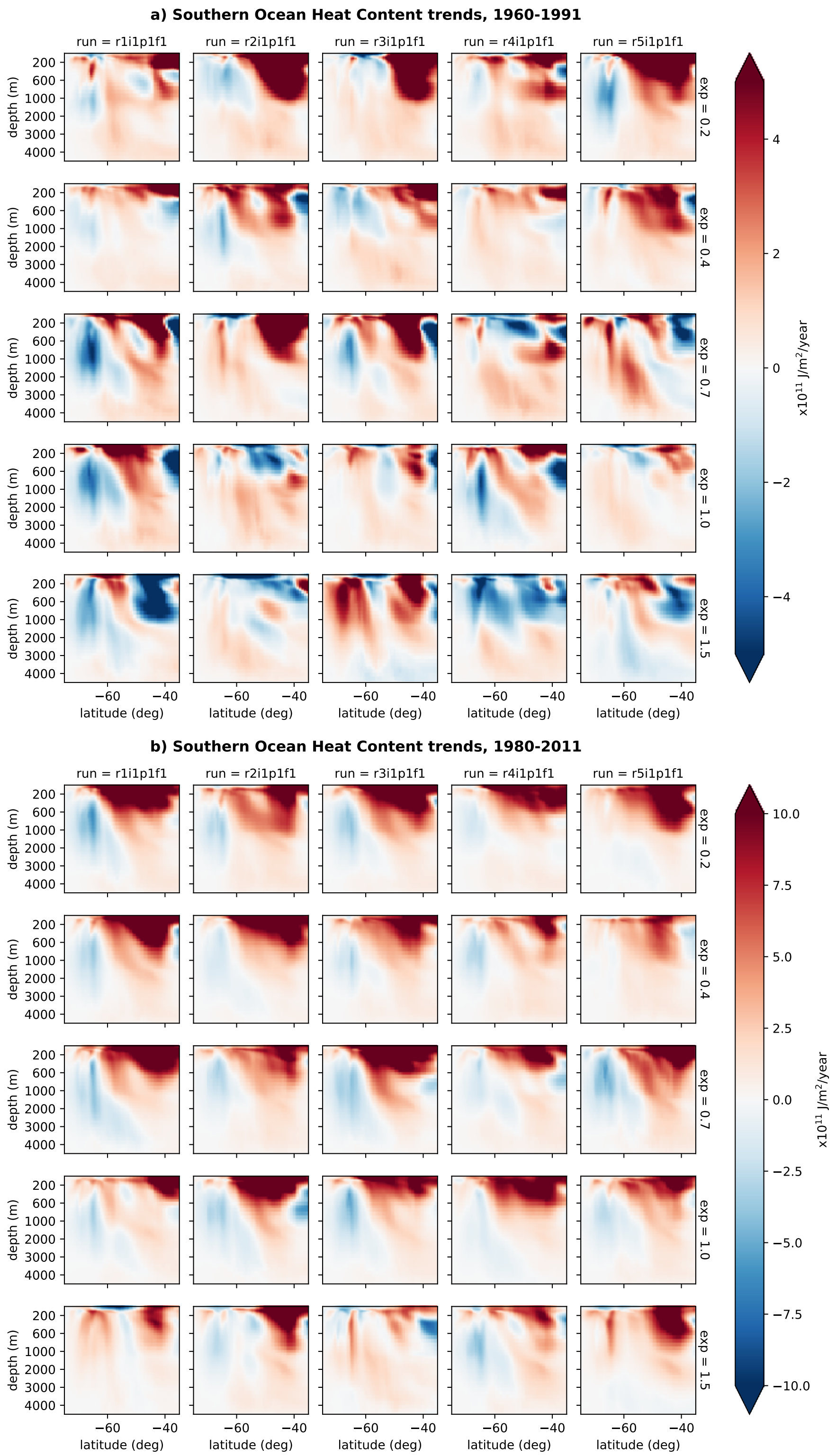

Figure S7. As in figure S3, except for the Southern Ocean.

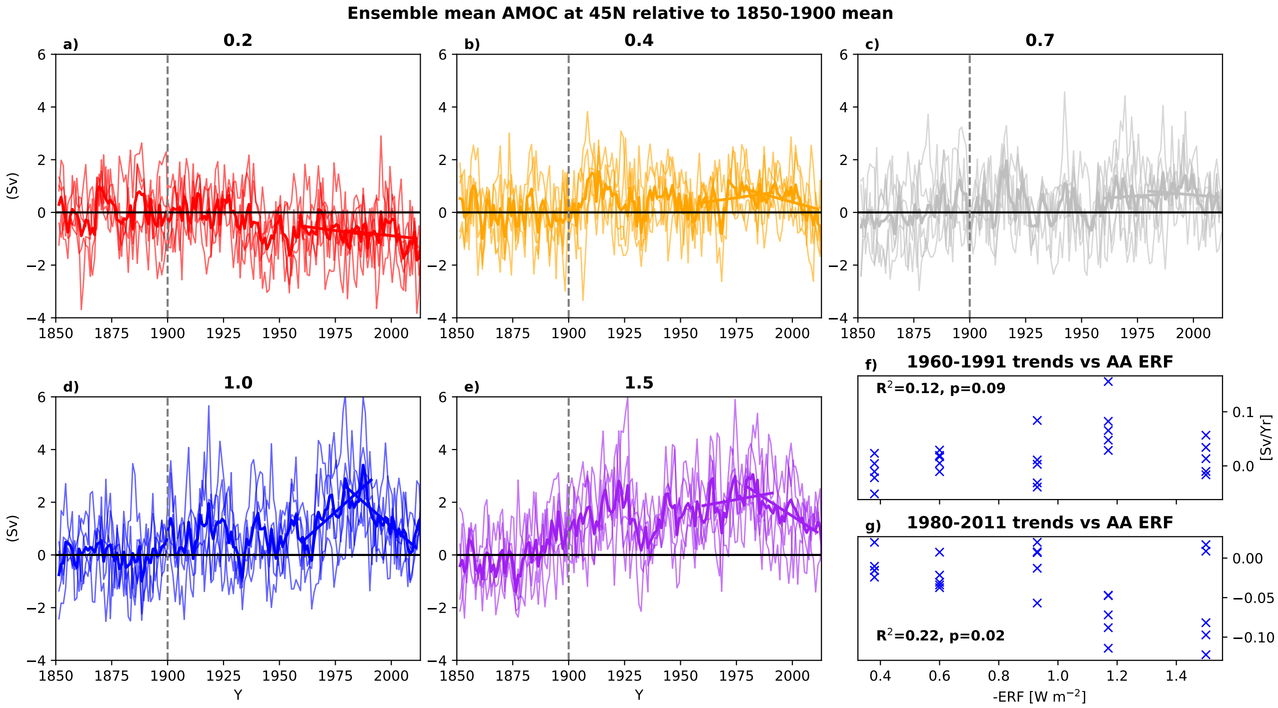

Figure S8. Panels a-e show the AMOC at 45N relative to the 1850-1900 mean, for each forcing factor as labeled. Thin lines are individual ensemble members and thicker lines are ensemble means. Straight thick lines indicate ensemble-mean linear trends over 1960-1991 and 1980-2011. Linear trends for all ensemble members are shown in panels f and g, plotted against AA ERF. R^2 and p are shown for the linear correlation of the trends against ERF magnitude.

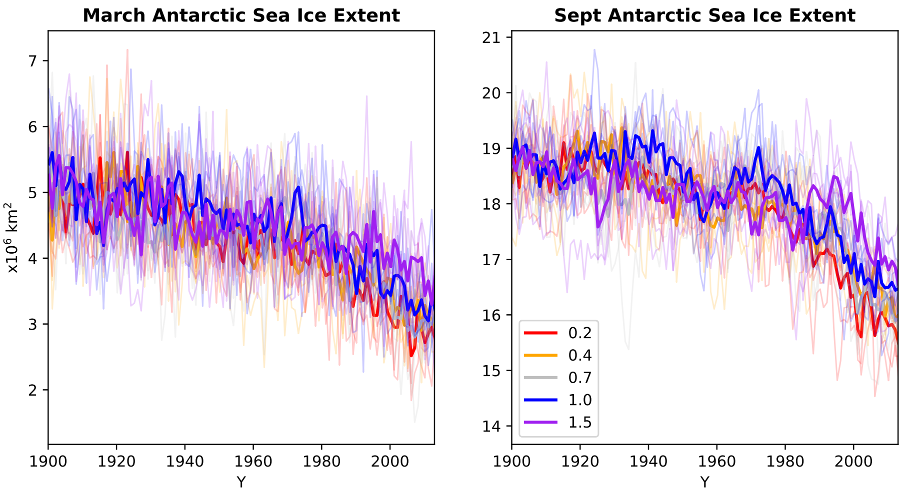

Figure S9. March and September Southern Hemisphere sea ice extent for each forcing factor as labelled. Thin lines are individual ensemble members and thicker lines are ensemble means.